Spin-isospin strength distributions in f-p shell nuclei:
A study of the ^{51}V(n,p) and ^{59}Co(n,p) reactions at 198 MeV

W. P. Alford,[1] B. A. Brown,[2] S. Burzynski,[3,*] A. Celler,[1] D. Frekers,[4]
R. Helmer,[4] R. Henderson,[4,5] K. P. Jackson,[4] K. Lee,[1] A. Rahav,[6] A. Trudel,[3]
and M. C. Vetterli[3,4]

[1] University of Western Ontario, London, Ontario, Canada N6A 3K7
[2] Department of Physics and Astronomy, Michigan State University, East Lansing, Michigan 48824
[3] Simon Fraser University, Burnaby, British Columbia, Canada V5A 1S6
[4] TRIUMF, 4004 Wesbrook Mall, Vancouver, British Columbia, Canada V6T 2A3
[5] University of Melbourne, Parkville, Victoria, Australia 3052
[6] Tel Aviv University, 69978 Ramat Aviv, Israel
(Received 1 June 1993)

The (n,p) reaction has been studied on the nuclei ^{51}V and ^{59}Co at an energy of 198 MeV. Spectra were measured at laboratory angles of 0°, 4°, 8°, 12°, 16°, and 20° up to an excitation energy of 35 MeV in the final nuclei ^{51}Ti and ^{59}Fe. A multipole analysis of the data up to 30 MeV was carried out to identify Gamow-Teller (GT) ($\Delta L = 0, \Delta J^\pi = 1^+$) and spin-dipole ($\Delta L = 1, \Delta J^\pi = 0^-, 1^-, 2^-$) strengths. GT strength is concentrated in a resonance with centroid energy of 5.2 MeV in ^{51}Ti and 4.1 MeV in ^{59}Fe. The spin-dipole strength appears as a broad resonance with centroid energy about 16 MeV in both nuclei. Shell model calculations of the GT strength reproduce the energy distribution reasonably well, but the calculated strength exceeds the measurement by a factor of about 4.

PACS number(s): 25.40.Kv, 24.30.Cz, 27.40.+z, 27.50.+e

I. INTRODUCTION

In recent years there has been extensive interest in the spin-isospin effective interaction and the corresponding nuclear response. Experimentally, the isospin character of the response may be defined by studying charge exchange reactions such as (p,n), (n,p), or $(^3$He$,t)$. Studies of the (p,n) reaction [1,2] have established that at intermediate energies (100–300 MeV) the spin-flip part of the effective interaction is much stronger than the non-spin-flip. Thus the study of charge exchange reactions at intermediate energies has provided a convenient and powerful probe of the spin-isospin response in nuclei.

For small momentum transfers the response is dominated by Gamow-Teller (GT) transitions, corresponding to $\Delta J^\pi = 1^+$ ($\Delta L = 0$, $\Delta S = 1$), which are readily identified by the strong peaking of the reaction cross section at 0°. At larger momentum transfers, corresponding to higher excitation energies or larger scattering angles, higher multipoles of the effective interaction become important and may be identified by the characteristic angular distributions associated with the angular momentum transfer of each multipole. In practice much of the transition strength arising from the lowest-order multipoles ($\Delta L = 0$ and 1) can be unambiguously identified. The existence of strength arising from higher multipoles is readily observable, but the measurement of strength arising from specific multipoles becomes increasingly uncertain as ΔL increases. At the same time, the identification of small components of transition strength for $\Delta L = 0$ or $\Delta L = 1$ becomes difficult or even impossible if that strength occurs in regions dominated by strength arising from other multipoles.

In spite of these limitations the study of (p,n) and (n,p) reactions at low excitation and forward angles provides a relatively clear measurement of GT($\Delta L = 0$, $\Delta J^\pi = 1^+$) and spin-dipole ($\Delta L = 1$, $\Delta J^\pi = 0^-,1^-,2^-$) transition strengths. For the spin-dipole transitions, measured angular distributions might provide identification of 0^- strength. It is not feasible to separate 1^- and 2^- transitions from each other on the basis of cross sections alone, but the data can give a reasonable estimate of the total $\Delta L = 1$ strength in such transitions.

In this work we have studied the (n,p) reaction on two (fp) shell nuclei, ^{51}V and ^{59}Co, which play a significant role in late stages of the evolution of massive stars, just prior to the presupernova collapse of the stellar core [3]. The cross section for GT transitions is directly proportional to the electron capture cross section [4] on these nuclei; this is an important ingredient in calculations of the reactions leading to the final collapse and possible supernova formation [5]. Electron capture may also occur via first forbidden beta transitions corresponding to the spin-dipole transitions observed in the (n,p) reaction. In addition to providing data of direct interest in the astrophysical calculations, the data are also important as a test of the nuclear model calculations which must be used to estimate electron capture rates on nuclei, such as unstable species, which are not available for direct experimental studies.

*On leave from Institute for Nuclear Studies, Swierk, Poland.

II. EXPERIMENTAL DETAILS

Measurements were carried out using the TRIUMF charge exchange facility in the (n,p) mode. The essential components of the facility are shown in Fig. 1, and described in more detail in Ref. [6]. Neutrons are produced in the ^{7}Li(p,n) reaction with a proton beam of 200 MeV energy. In order to control the effect of energy spread in the proton beam, the beam can be momentum dispersed across the ^{7}Li strip target, the width of which determines the beam energy spread on the target. The reaction excites the ground and 0.43 MeV excited states of ^{7}Be with comparable intensity, and the width of the target strip was usually chosen so that beam energy spread on the target was about 400 keV. In addition to the transitions to the two bound states in ^{7}Be, at 0° the reaction produces a continuum of neutrons up to at least 60 MeV excitation with an intensity of about 1%/MeV of the intensity of the sum of the transitions to the discrete bound states. Beam currents were typically 300–400 nA, and produced a neutron flux of about 10^5 neutron/cm^2 s on targets 2 cm × 5 cm in area.

Targets were metal foils mounted in a target box [7] which allows up to six targets to be mounted between proportional wire chamber planes. Protons from the (n,p) reaction produce a signal in each wire chamber plane downstream of the target in which the reaction occurs. The resulting hit pattern identifies the target involved in each event, and permits software corrections to be made for energy loss in subsequent targets. The
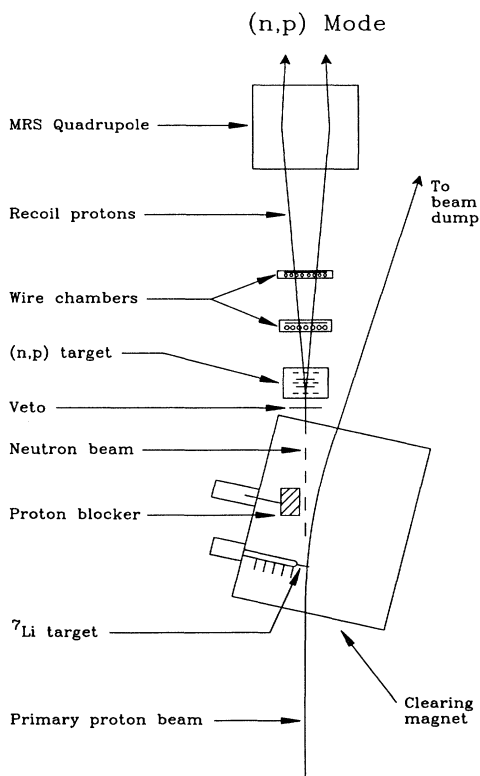
(n,p) Mode

FIG. 1.   Schematic layout of the TRIUMF (n,p) facility.

reaction protons then traverse two sets of drift chambers (the front-end counters) which measure the position and direction of each proton as it leaves the target stack. Protons then enter the medium resolution spectrometer (MRS) where they are momentum analyzed and detected by a series of counters at the exit.

The measured spectra extended to an excitation energy of about 35 MeV, and were recorded at MRS angles of 0°, 4°, 8°, 12°, 16°, and 20°.

In measurements reported here, the first target was of natural carbon 147 mg/cm^2 in thickness, and the sixth target was polyethylene (CH$_2$) 44 mg/cm^2 in thickness. The CH$_2$ target provided a calibration of the cross section in each measurement from observation of the proton peak from the ^{1}H(n,p) reaction. The cross section for this reaction was calculated from measured (n,p) phase shifts using the program SAID (SM90) [8]. The carbon target provided a reference spectrum for the ^{12}C(n,p) reaction which was subtracted from the CH$_2$ target spectrum in order to obtain the spectrum of incident neutrons from the ^{7}Li(p,n) reaction. The vanadium targets consisted of four foils of 99.5% purity with thickness 234, 156, 156, and 77.9 mg/cm^2. The cobalt targets were four foils of 99.99% purity with thicknesses 225, 225, 86.2, and 86.2 mg/cm^2. All targets were approximately 5.0 cm × 2.5 cm in area.

In addition to these target stacks, two others were used. One consisted of six CH$_2$ targets which was used to measure the relative neutron flux and proton detection efficiency for different target positions. The second consisted of five empty positions with a CH$_2$ target in the last position, which could be used to monitor background and with an external CH$_2$ target to check the efficiency of the target box wire counters.

Since the acceptance of the MRS depends upon position in the focal plane, this was determined by measuring relative counting rates for protons from the ^{1}H(n,p) reaction as a function of magnetic field setting in the MRS. For this measurement, the incident proton beam was focused achromatically on a ^{7}Li target about 1.5 cm high so that the full beam was intercepted by the target, and beam charge was integrated in a Faraday cup, with an accuracy of 3%. This measurement also provided the data for the calibration of energy as a function of focal plane position. In the measurements, this calibration was used to establish excitation energies in each measurement relative to an origin fixed by the proton group from the ^{1}H(n,p) reaction in the CH$_2$ target. Excitation energies were estimated to have an uncertainty of less than 100 keV.

III. DATA ANALYSIS AND RESULTS

Data were recorded event by event, and a fraction of the data was analyzed on line to monitor the progress of the measurements. Final data analysis was carried out off line using the program LISA.

A raw spectrum for the ^{51}V target at a MRS angle of 0° is shown in Fig. 2(a). The overall resolution was about 900 keV, measured by the width of the peak from the ^{1}H(n,p) reaction on the CH$_2$ target. The promi-
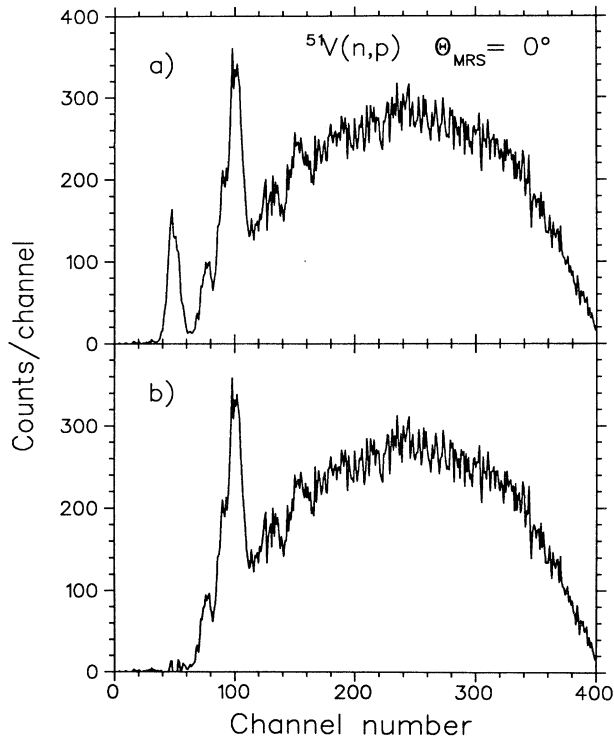
FIG. 2. (a) Raw spectrum for the ^{51}V target measured at an MRS angle of 0° (upper panel). (b) Spectrum after background subtraction (lower panel).

nent peak at the left side of the spectrum arises from the ^{1}H(n,p) reaction on hydrogen in the cathode planes of the wire counters plus a small amount of hydrogen absorbed on surfaces within the target box. In addition to this peak, there was a small background from other components in the wire chambers. The spectrum after background subtraction is shown in Fig. 2(b), and it is seen that except for the hydrogen peak the spectra are not affected within the statistical uncertainties of the data. Measurements were carried out at MRS angles of 0°, 4°, 8°, 12°, 16°, and 20°. The angular acceptance of the spectrometer was about ± 2°, and the actual distribution of events over this range was measured in the data analysis. The mean scattering angles in the center of mass system corresponding to the MRS positions were 1.7°, 4.7°, 8.6°, 12.6°, 16.6°, and 20.7°.

After background subtraction the spectra were corrected for spectrometer acceptance and for the effect of the continuum in the neutron source spectrum. The latter correction required a deconvolution using the measured energy spectrum of the neutron source. This correction was negligible at low excitation, but resulted in a decrease of about 30% in the spectra at 30 MeV excitation. The final corrected data were then binned in 1 MeV intervals to produce the spectra shown in Figs. 3(a),(b).

The measured energy distributions of Fig. 3 show a strong peak near 5 MeV excitation at the smallest angle (1.7° c.m.) which indicates the presence of GT transition strength. At 4.7° and 8.6° there is a broad peak be-
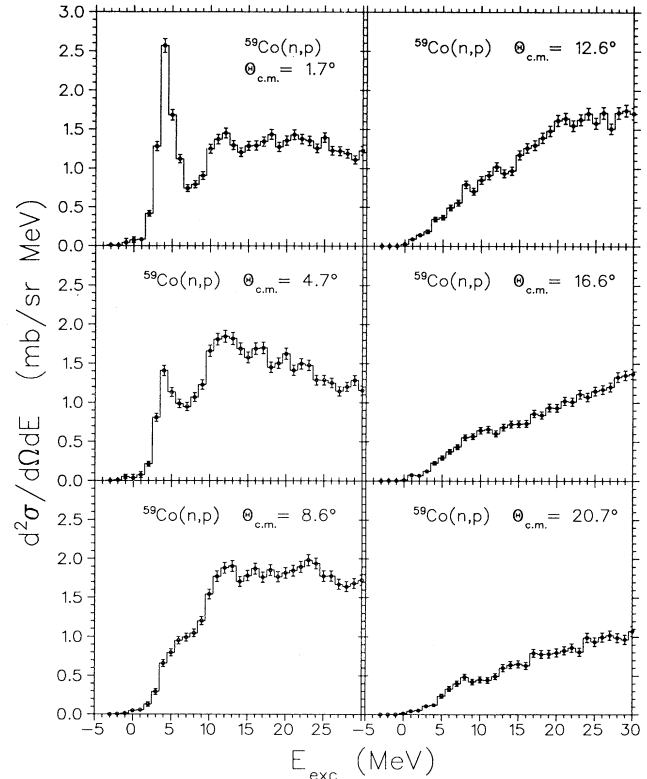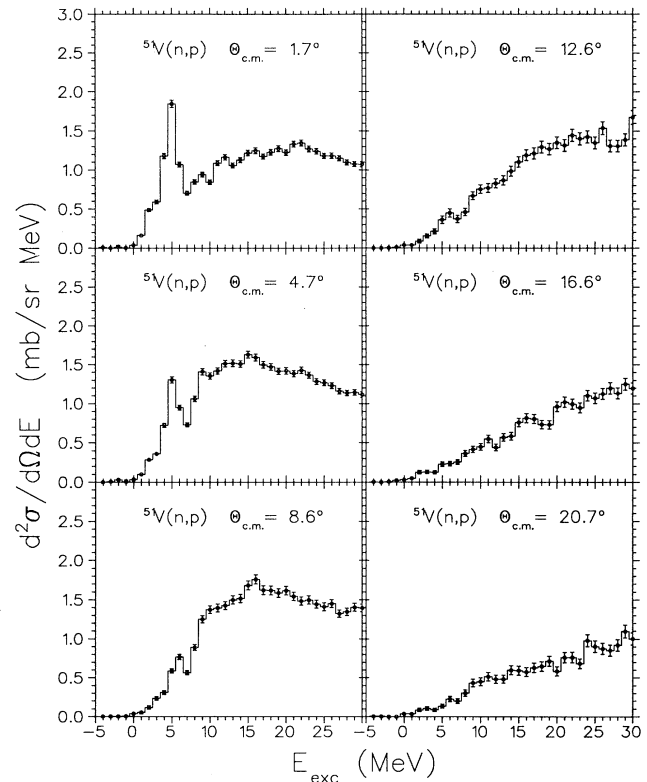

FIG. 3. (a) Binned spectra at each angle for the ^{51}V target plotted as a function of excitation energy in the final nucleus ^{51}Ti. (b) Binned spectra at each angle for the ^{59}Co target.

tween 15 and 20 MeV excitation arising from transitions to the spin-dipole giant resonance (SDGR). At larger angles there is no obvious structure indicating resonances arising from transitions with $\Delta L > 1$, though the magnitude of the cross section at high excitation indicates that such transitions must be important.

In order to obtain quantitative estimates of the different contributions to the cross section, a multipole analysis was carried out, assuming that the measured angular distributions could be fitted by a sum of shapes obtained from distorted wave impulse approximation (DWIA) calculations for a limited range of L and J transfers expected to be important. In the present experiment, it would be expected that significant contributions could arise for $\Delta L = 0$, $\Delta J^\pi = 1^+$; $\Delta L = 1$, $\Delta J^\pi = 0^-,1^-,2^-$; $\Delta L = 2$, $\Delta J^\pi = 1^+,2^+,3^+$; $\Delta L = 3$, $\Delta J^\pi = 2^-,3^-,4^-$; and possibly $\Delta L = 4$, $\Delta J^\pi = 3^+,4^+,5^+$. The measured cross section is then represented as

$$\sigma_{\text{expt}} = \sum_{\Delta J^\pi} C_{\Delta J^\pi} \sigma_{\text{DW}}(\Delta J^\pi) . \qquad (1)$$

The coefficients $C_{\Delta J^\pi}$ are determined by carrying out a least-squares fit of the calculations to the measured angular distribution for each energy bin in the spectra of Fig. 3.

It is important to recognize that since data are available at only six angles, the multipole analysis can include at most five terms in the sum. Thus it is necessary to determine whether such a limited number of terms can provide a resonable representation of the contributions expected to be important in the sum. This question is addressed in the following discussion of DWIA calculations.

A. DWIA calculations

All calculations were carried out using the DWIA code DW81 [9], which requires as input the optical potentials in the entrance and exit channels, a specification of single-particle states in the initial and final nuclei, a transition amplitude between initial and final states for a given value of ΔJ^π, and an effective interaction between the incident neutron and target nucleons.

In the present analysis the Franey-Love interaction [10] was taken to represent the effective interaction. The optical potentials were then generated by folding the Franey-Love effective interaction with a nuclear matter distribution using the program MAINX8 [11]. A few calculations were carried out with two other choices of optical potentials. One was a microscopic potential generated with MAINX8 using a density-dependent interaction, and the other was an empirical Woods-Saxon potential used in an earlier analysis of (n,p) measurements at 300 MeV [12]. For a given particle-hole transition amplitude it was found that the shapes of the angular distributions in the angular region near the maximum of the cross section were not affected by the choice of potentials, though the magnitude of the peak cross section showed a variation of as much as 50% for different choices. Since only the shapes of the angular distribution are significant in the multipole analysis however, such variation is not important, so that our results are insensitive to the choice of

optical potentials.

The single-particle states involved in the transition amplitude were taken as harmonic oscillator states with oscillator parameter $b = 1.9$ fm.

Since realistic shell model wave functions were not available, it was necessary to assume that the angular distributions required in the analysis could be calculated using transition amplitudes for a single particle-hole configuration for each value of ΔJ^π. In order to support this assumption a series of calculations was carried out to investigate the sensitivity of the calculated DWIA shapes to the assumed transition amplitude. For transitions involving no change in parity ($\Delta L = 0, 2, 4$) calculations were carried out for a number of transition amplitudes involving excitations of either $0\hbar w$ or $2\hbar w$. For transitions involving a parity change ($\Delta L = 1, 3, 5$) only excitations of $1\hbar w$ were considered. In comparing results for a given ΔJ^π, it is helpful to recognize that for unnatural parity transitions with $\Delta J \geq 1$ the calculated cross section may include contributions from two different values of the orbital angular momentum transfer, namely, $\Delta L = \Delta J \pm 1$. Thus it may be expected that such transitions will show a greater sensitivity to choice of transition amplitude than will the natural parity transitions which have only a single orbital momentum contribution with $\Delta L = \Delta J$.

A summary of the results of these calculations follows.

1. $\Delta J^\pi = 1^+$

These transitions are of primary interest, since they include the GT strength. In the simplest shell model description of ^{51}V and ^{59}Co, the valence protons occupy the $f_{7/2}$ orbit and the neutron $f_{7/2}$ orbit is completely filled. The only neutron state available for $0\hbar w$ GT transitions is then $f_{5/2}$, so that it was assumed that the angular distribution of the cross section for GT transitions could be adequately modeled with a transition to the $(\pi f_{7/2})^{-1} (\nu f_{5/2})$ configuration. Configuration mixing in the ground state would allow transitions to configurations such as $(\pi f_{7/2})^{-1} (\nu f_{7/2})$ or $(\pi p_{3/2})^{-1} (\nu p_{1/2})$, but such amplitudes are expected to be relatively small, and angular distributions for these transitions are very similar to that for the dominant $(\pi f_{7/2})^{-1} (\nu f_{5/2})$ configuration.

Transitions with $\Delta J^\pi = 1^+$ are also expected at higher excitation energies as a result of $2\hbar w$ excitations. Such transitions are not part of the GT strength, but represent isovector monopole excitations. Calculated angular distributions for transitions to several possible configurations showed a wide variety of shapes, with no single characteristic shape such as is found for GT transitions. For transitions to configurations with no change in the single-particle orbital angular momentum, such as $(\pi 0d_{5/2})^{-1} (\nu 1d_{3/2})$, angular distributions peaked at $0°$ with a strong secondary maximum near $15°$, and might be represented as a sum of cross sections for a GT transition plus $\Delta J^\pi = 2^+$. For transitions with $\Delta L = 2$, involving configurations such as $(\pi 1s_{1/2})^{-1} (\nu 1d_{3/2})$, angular distributions peaked near $7°$, and resembled those expected for $\Delta J^\pi = 1^-$. It was concluded that it would not be feasible to include such contributions in the mul-

tipole analysis, and it is unlikely that they could be unambiguously identified in any case.

2. $\Delta J^\pi = 2^+$

At low excitation energy these transitions would arise mainly from the $0\hbar w$ transition to the $(\pi 0 f_{7/2})^{-1} (\nu 0 f_{5/2})$ configuration with possible small contributions from configurations, such as $(\pi 1 p_{3/2})^{-1} (\nu 0 f_{5/2})$, associated with core excitations in the target. The angular distributions for these transitions show a characteristic shape with a peak near $11.5°$. At higher excitation, many transitions can arise from $2\hbar w$ excitations which show angular distributions similar to those for the $0\hbar w$ transitions, with peak cross sections at $10°$ to $11.5°$. It was therefore concluded that angular distributions for all $\Delta J^\pi = 2^+$ transitions could be adequately modeled using the DWIA results for the transition to the $(\pi 0 f_{7/2})^{-1} (\nu 0 f_{5/2})$ configuration.

3. $\Delta J^\pi = 3^+$

Transitions of this character arise at low excitation from most of the $0\hbar w$ single-particle transitions which also allow $\Delta J^\pi = 2^+$. For the $(\pi 0 f_{7/2})^{-1} (\nu 0 f_{5/2})$ configuration the angular distribution for $\Delta J^\pi = 3^+$ is similar in shape to that for $\Delta J^\pi = 2^+$ but the peak cross section is shifted by $2°$ from $11.5°$ to $13.5°$. For $2\hbar w$ excitations, the calculated angular distributions exhibit peak cross sections at angles ranging from $10°$ to $22°$, with no single characteristic shape. As a rough approximation, the angular distributions could be modeled as a sum of those for $0\hbar w$ transitions with $\Delta J^\pi = 2^+$ and $\Delta J^\pi = 4^+$.

4. $\Delta J^\pi = 0^-$

Since transitions involving a parity change require single-particle excitations of at least $1\hbar w$, it is expected that most of the strength for such transitions will be at excitation energies well above the GT resonance. Random phase approximation (RPA) calculations [13] for ^{60}Ni(n,p) indicate that the centroid of the strength for $\Delta J^\pi = 0^-$ transitions lies at 18.9 MeV with respect to the parent ground state or 16.1 MeV relative to the ^{60}Co ground state. In a lowest-order shell model, single-particle configurations closest to the Fermi surface that contribute to transitions with $\Delta J^\pi = 0^-$ are $(\pi 1 s_{1/2})^{-1} (\nu 1 p_{1/2}), (\pi 0 d_{5/2})^{-1} (\nu 0 f_{5/2})$ and in ^{51}V, $(\pi 0 d_{3/2})^{-1} (\nu 1 p_{3/2})$. At somewhat higher excitation the $(\pi 0 f_{7/2})^{-1} (\nu 0 g_{7/2})$ configuration could also become important. The DWIA angular distributions for all these transition amplitudes are almost identical in shape, with a maximum cross section between $4.5°$ and $5°$. Thus $\Delta J^\pi = 0^-$ transitions are expected to show a well-defined, characteristic angular distribution.

5. $\Delta J^\pi = 1^-$

For these transitions, the single-particle configuration closest to the Fermi surface is $(\pi 0 f_{7/2})^{-1} (\nu 0 g_{9/2})$, with many other possibilities such as $(\pi 1 s 0 d)^{-1} (\nu 1 p 0 f)$ or

$(\pi 1 p 0 f)^{-1} (\nu 2 s 1 d 0 g)$ at somewhat higher energies. DWIA calculations showed that most of these transitions gave rise to angular distributions very similar to that for the $(\pi 0 f_{7/2})^{-1} (\nu 0 g_{9/2})$ configuration, with a peak cross section near $6.5°$. It was concluded that the calculated cross section for this latter transition amplitude provided a characteristic angular distribution for all $\Delta J^\pi = 1^-$ transitions in the region of excitation of interest in this analysis.

6. $\Delta J^\pi = 2^-$

Most configurations giving rise to $\Delta J^\pi = 1^-$ transitions also allow transitions with $\Delta J^\pi = 2^-$. It was found that calculated cross sections for $\Delta J^\pi = 2^-$ showed more variability than for $\Delta J^\pi = 1^-$, though angular distributions for most transitions with large cross sections were quite similar to that for the transition to the $(\pi 0 f_{7/2})^{-1} (\nu 0 g_{9/2})$ configuration for $\Delta J^\pi = 1^-$. Because of the need to limit the number of DWIA shapes in the multipole analysis, it was assumed that transitions for $\Delta J^\pi = 2^-$ could be modeled adequately by the angular distribution for the transition to the $(\pi 0 f_{7/2}) (\nu 0 g_{9/2})$ configuration with $\Delta J^\pi = 1^-$, plus a possible contribution from the $\Delta J^\pi = 3^-$ distribution described below.

7. $\Delta J^\pi = 3^-$

DWIA calculations were carried out for a large number of transitions to configurations previously considered for $\Delta J^\pi = 1^-$ and 2^-. For $\Delta J^\pi = 3^-$ the angular distributions were all generally similar to one another with a broad peak centered at an angle between $13.5°$ and $16.5°$ for different configurations. It was concluded that the calculated angular distribution for the transition to the $(\pi 0 f_{7/2})^{-1} (\nu 0 g_{9/2})$ configuration provided a reasonably "typical" shape for all $\Delta J^\pi = 3^-$ transitions.

8. $\Delta J^\pi = 4^-$

Calculated angular distributions for these transitions were qualitatively similar to those for $\Delta J^\pi = 3^-$, with peak cross sections occurring at an angle between $14.3°$ and $18.3°$ for different configurations. Although the angular distributions show somewhat more variability than those for $\Delta J^\pi = 3^-$ with peak cross sections at slightly larger angles, it was concluded that the "typical" shape for $\Delta J^\pi = 3^-$ would give a reasonable average representation for $\Delta J^\pi = 4^-$ transitions also.

B. Multipole analysis

From the results of the DWIA calculations for different simple particle-hole transitions, it appeared that except for $\Delta J^\pi = 0^-$ the angular distributions were characteristic of the orbital angular momentum transfer ΔL rather than ΔJ^π. Much of the variability for transitions of unnatural parity could be approximately represented by a sum of angular distributions for the two values of $\Delta L (= \Delta J \pm 1)$ allowed in such transitions. For

this reason it was concluded that the multipole analysis should be based on the four characteristic or "average" shapes obtained for natural parity transitions with $\Delta L = 1, 2, 3$ plus the $\Delta J^\pi = 1^+$ shape predicted for the $(\pi 0 f_{7/2})^{-1} (\nu 0 f_{5/2})$ configuration. The calculated shapes for an excitation energy of 15 MeV in the $^{51}V(n,p)$ reaction are shown in Fig. 4.

The multipole analysis program [14] carried out a least-squares fit of the measured angular distribution in each 1 MeV bin to a sum of these shapes as indicated in Eq. (1). Shapes were calculated at intervals of 10 MeV between excitation energies from -5 MeV to 35 MeV, and predicted shapes were then interpolated to the actual excitation energy for each angular distribution. For each ΔL the same particle-hole configuration was assumed throughout the full range of excitation energies, so that the only energy dependence comes from the distortion and kinematic effects of the DWIA.

The results of the fit to the measured angular distributions for several 1 MeV energy bins are shown in Fig. 5 for the vanadium data. At an excitation energy of 5 MeV, the angular distributions show strong forward peaking, indicating the importance of GT transitions in the cross section. At 10 and 15 MeV excitations, the spin-dipole ($\Delta L = 1$) cross section dominates the angular distributions, while at 25 MeV, $\Delta L = 3$ transitions make the largest contribution. It is noteworthy that while a $\Delta L = 2$ shape was included in the fit, the contribution of this shape is negligible.

At excitation energies above 5 MeV, the fit requires a small contribution with $\Delta L = 0$, although the measured angular distributions do not show any forward peaking. The uncertainty in this contribution is large, mainly as the result of uncertainties in the details of the shape of the angular distribution for $\Delta L = 1$. The location of the peak cross section for $\Delta L = 1$ transitions is not very sensitive to the particular particle-hole configuration assumed or to the choice of optical potentials, but the ratio of peak cross section to that at $0°$ does show significant dependence on these quantities. Since the $\Delta L = 0$ component at high excitation is determined mainly by the measured cross section at the smallest angle, $1.7°$, it is
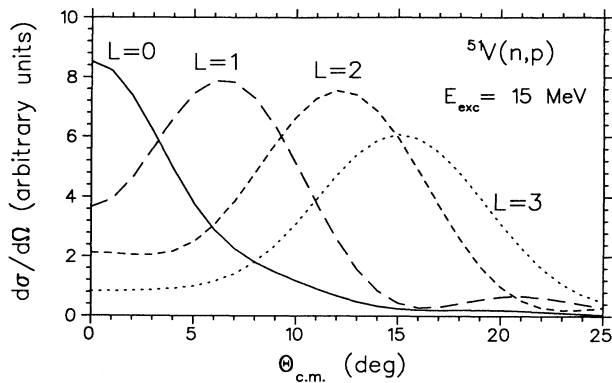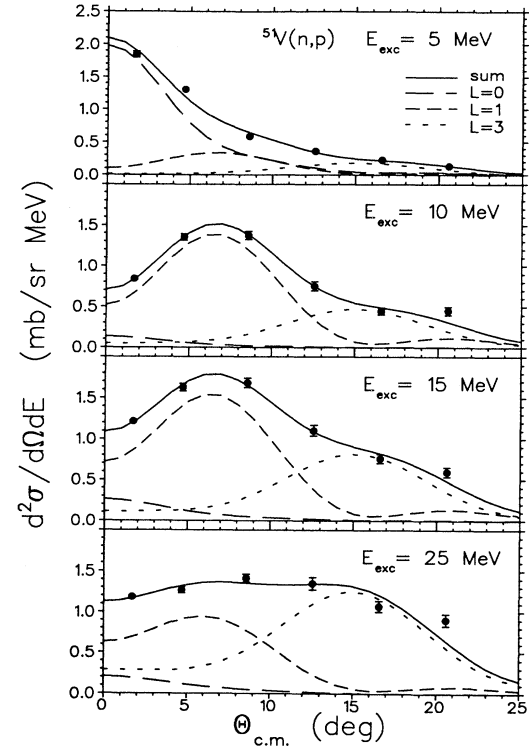

FIG. 5. Fits to measured angular distributions from $^{51}V(n,p)$ for 1 MeV bins at excitation energies of 5, 10, 15, and 25 MeV. The individual components from the multipole analysis are shown along with the summed cross section (solid line). Note that no significant contribution is found for $L = 2$.

possible that much of this component reflects the uncertainty in the precise shape of the angular distribution for $\Delta L = 1$ transitions rather than true $\Delta L = 0$ transition strength.

It is also seen that the data at high excitation at $20.7°$ is consistently greater than the calculated cross section, indicating the importance of transition strength with $\Delta L > 3$.

The multipole decomposition for the measured spectrum at each angle is shown in Fig. 6 for the $^{51}V(n,p)$ reaction. At forward angles, the fit to the data is generally good. However, the analysis consistently yields too small a cross section at $20.7°$ for excitation energies above 5 MeV, and too large a cross section at $16.6°$ for energies above 15 MeV. Both of these failures are an indication of the importance of contributions with $\Delta L > 3$ at large angles, as noted previously.

A second representation of these results is displayed in Fig. 7, which shows the energy distribution of the contribution to the total cross section for each value of ΔL. In this case, each contribution is shown for the measured angle closest to the peak of the calculated cross section for that particular contribution. The error bars shown in Fig. 7 represent the uncertainty in the fits arising from uncertainties in the data only. Systematic uncertainties arising from the differences in DWIA angular distributions for different transition amplitudes are discussed below.
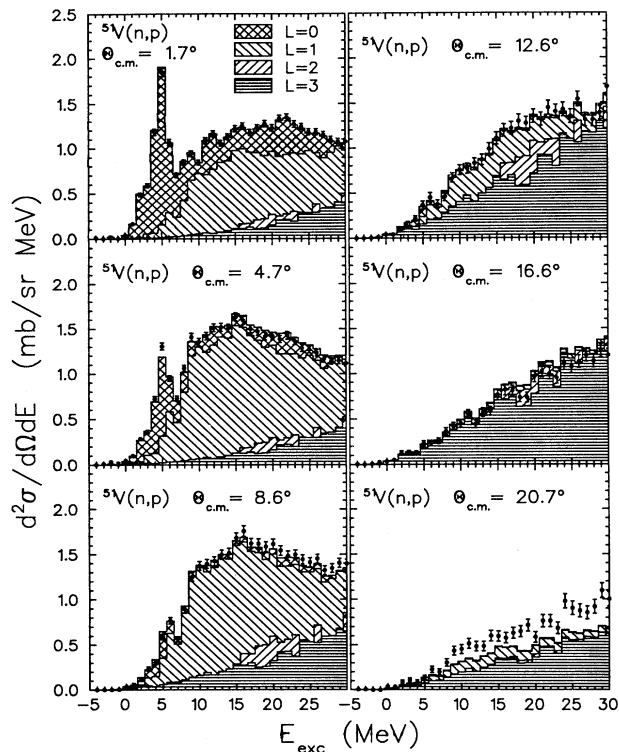

FIG. 4. DWIA shapes used for the multipole decomposition of $^{51}V(n,p)$ data. Calculations are shown for an excitation energy of 15 MeV in the final nucleus.

FIG. 6. Results of the multipole decomposition for the ^{51}V(n,p) data. At each angle, the contribution of each of the four assumed components is shown. Error bars on the data points represent statistical uncertainties.
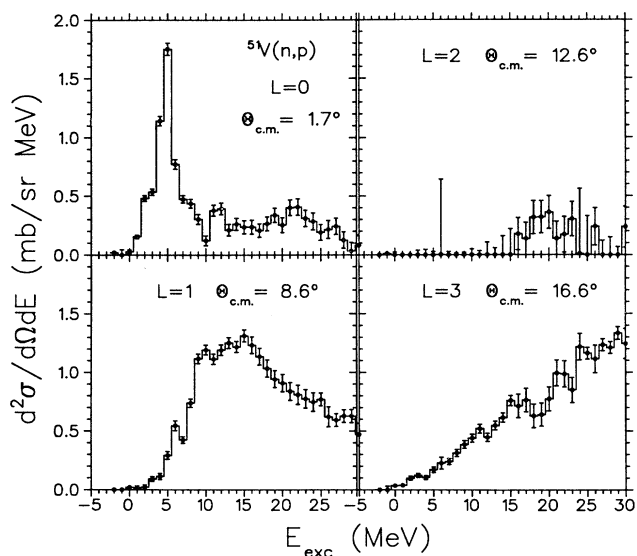

FIG. 7. Energy dependence of the partial cross sections for $L = 0$, 1, 2, and 3 components of the multipole decomposition of the data in Fig. 6. The cross section is shown for a c.m. angle of 1.7° for $L = 0$, 8.6° for $L = 1$, 12.6° for $L = 2$, and 16.6° for $L = 3$. These are the measured angles closest to the maximum angle predicted by the DWIA calculations. The error bars shown arise from both statistical uncertainties in the data and from the least-squares fitting in the multipole decomposition.

It is seen in Fig. 7 that the cross section for $\Delta J^\pi = 1^+$ exhibits a well-defined peak centered at 5.1 MeV, with a width [full width at half maximum (FWHM)] of about 2.5 MeV. In addition, the analysis indicates the presence of $\Delta J^\pi = 1^+$ strength over the full energy range of the data. As shown in Fig. 5, and discussed in that connection, the measured angular distributions at excitations above about 8 MeV do not show the forward peaking which provides an unambiguous signature of $\Delta J^\pi = 1^+$ transitions. In this situation it must be concluded that while such transitions may be present, the present analysis provides only a qualitative estimate of their possible magnitude.

The energy dependence of the cross section for transitions with $\Delta L = 1$ shows a resonancelike behavior with maximum cross section at an excitation energy of 15 MeV and FWHM of about 15 MeV. There is also some indication of structure near 6 MeV and 12 MeV excitation. The mean energy is 17.1 MeV. Analyses with different transition amplitudes for $\Delta L = 1$ and 3 were carried out which showed that the $\Delta L = 1$ cross section was insensitive to the choice of transition amplitudes for excitation energies up to 20 MeV, with a variability of about ±25% at 30 MeV. The energy-integrated cross section up to 30 MeV was equal to 23 mb/sr at 8.6°. This result varied by less than 10% for the different choices of transition amplitudes, and should provide a reliable estimate of the total spin-dipole transition strength.

For transitions with $\Delta L = 2$ the multipole analysis using the DWIA result for a transition to the $(\pi 0f_{7/2})^{-1} (\nu 0f_{5/2})$ configuration shows no significant contribution to the measured cross section. This result is quite sensitive to the choice of transition amplitude for $\Delta L = 3$ however. With the assumption of a transition to the $(\pi 0d_{3/2})^{-1} (\nu 0f_{5/2})$ configuration for $\Delta J^\pi = 3^-$, the calculated peak cross section occurred at an angle of 16.5°, about 1.5° greater than for the "standard" shape used in the present analysis. A multipole analysis with this second shape showed that nearly half the cross section which had been identified as $\Delta L = 3$ in the original analysis was now identified as $\Delta L = 2$ at angles of 12° or less, although estimates of GT and spin dipole cross section were not changed. Such sensitivity to the choice of transition amplitude means that systematic uncertainties are large and poorly defined for the estimates of cross section contributions for both $\Delta L = 2$ and $\Delta L = 3$. Although the sum of the contributions for $\Delta L \geq 2$ is well determined, the individual components are not.

The cross section shown for $\Delta L = 3$ actually provides an estimate of contributions for all components with $\Delta J \geq 3$. In the light of difficulty of separating contributions from $\Delta L = 2$ and $\Delta L = 3$, however, it was concluded that it was not useful to attempt a more detailed decomposition for angular momentum transfers greater than for the spin dipole transitions.

Results of the multipole analysis for ^{59}Co(n,p) are shown in Figs. 8 and 9. The energy dependence of the cross sections for the four components assumed in the analysis is very similar to that found for the ^{51}V target. The systematic uncertainties in the results arising from the choice of transition amplitudes were also similar.
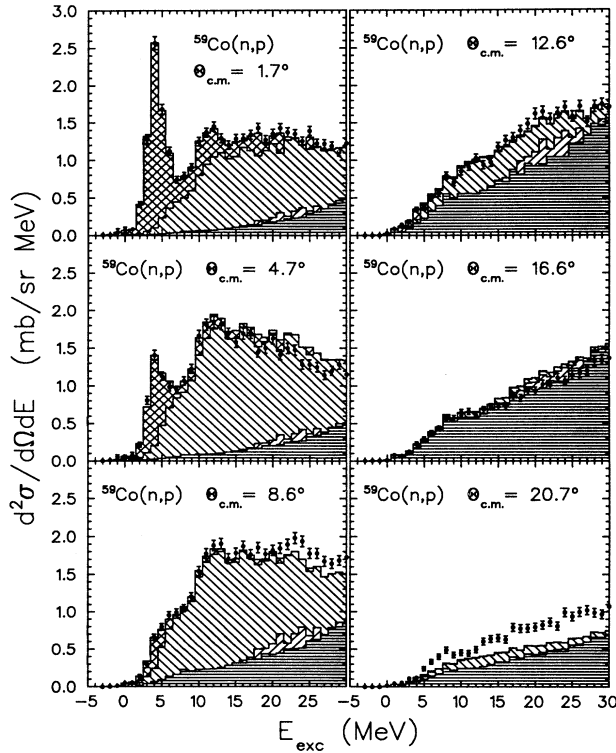
FIG. 8. Results of the multipole decomposition for the ^{59}Co(n,p) data. At each angle the contribution of each of the four assumed components is shown, using the same identification as in Fig. 6. Error bars on the data points represent statistical uncertainties.
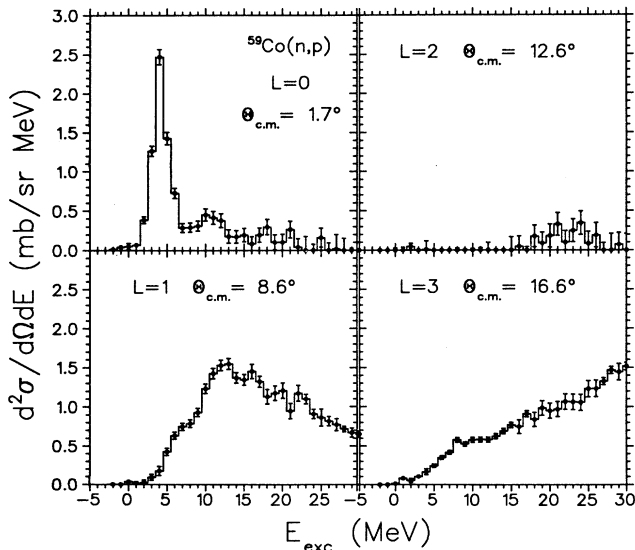

FIG. 9. Energy dependence of the partial cross sections for $L = 0$, 1, 2, and 3 components of the multipole decomposition of the ^{59}Co(n,p) data shown in Fig. 8. See caption to Fig. 7.

The most significant difference between the results for the two targets is in the magnitude and location of the GT strength, with somewhat greater strength in ^{59}Co, at a centroid energy about 1 MeV less than for ^{51}V.

The energy dependence of the cross section for $\Delta L = 1$ transitions was similar to that for ^{51}V with a mean energy of 16.9 MeV and a total cross section at 8.6° of 27 mb/sr, up to an excitation energy of 30 MeV.

IV. DISCUSSION

A. GT strength distributions

The distribution of GT strength connecting the ground state of each target to states in the final nucleus has been estimated from the measured $\Delta L = 0$ cross sections. To do this, the measured cross sections at 1.7° were extrapolated to zero momentum transfer ($0=0°$, $\Delta q = 0$) using DWIA calculations as described in the multipole analysis. These extrapolated cross sections were then converted to GT strength [in units for which $B_{GT}(n \to pe\bar{\nu}) = 3$] using values of the reduced cross section $\hat{\sigma} = \frac{\sigma(q=0)}{B_{GT}}$ obtained by interpolation from measurements of (p, n) cross sections [1, 15] for transitions between states of known beta decay strength. The values used were $\hat{\sigma}$=4.60 mb/sr for ^{59}Co and 5.44 mb/sr for ^{51}V.

As noted above, the identification of $\Delta L = 0$ cross sections becomes increasingly uncertain above about 8 MeV because of uncertainties in the DWIA shapes required in the multipole analysis. Since GT strength arises from $0\hbar w$ transitions, it is expected to be located at low excitation energy, largely below the $\Delta L = 1$ strength which arises from $1\hbar w$ excitations. Some GT strength may however be shifted to higher energies as a result of mixing with 2p-2h (two-particle–two-hole) excitations induced by short range correlations and the tensor interaction [16, 17]. Furthermore, $2\hbar w$ transitions may also give rise to cross sections with a $\Delta L = 0$ component at high excitations. In the light of these uncertainties it was concluded that 8 MeV was a reasonable upper limit on the energy at which GT strength could be reliably related to measured $\Delta L = 0$ cross sections. The resulting strength distributions are shown in Fig. 10 for ^{51}V and Fig. 11 for ^{59}Co. The total GT strength up to 8 MeV was 1.2 ± 0.1 units for ^{51}V and 1.9 ± 0.1 units for ^{59}Co.

Shell model calculations for comparison with these results were carried out using the program OXBASH [18]. These calculations used truncated vector spaces which are shown in Table I. The effective interaction was one which has recently been obtained by Brown [19] from a fit to 494 known binding energies and excitation energies in the mass region $A = 41 - 66$.

In order to account for uncertainties in the calculations and to simulate the finite energy resolution in the measurements, the strength of each discrete state in the calculation was spread over a Gaussian distribution with FWHM of 1.5 MeV. The resulting continuous distribution was then summed in bins of 1 MeV width for comparison with the data, and the total calculated strength was renormalized to be equal to the measured strength up to 8 MeV excitation. The renormalization factor required
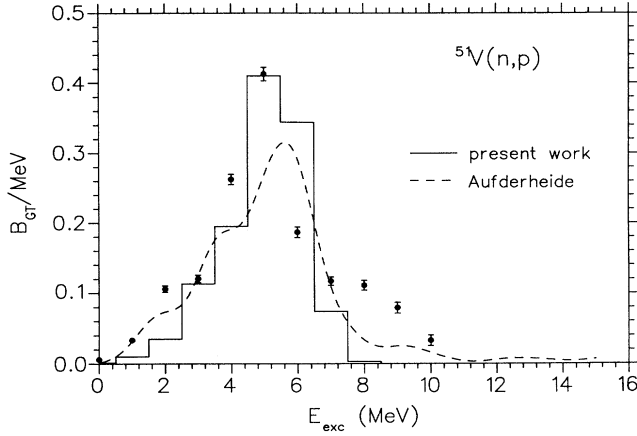
FIG. 10. Comparison of the measured GT strength distribution with model predictions for ^{51}V. The histogram is the result of calculations described in the text, and the curve is the result of calculations by Aufderheide [20].
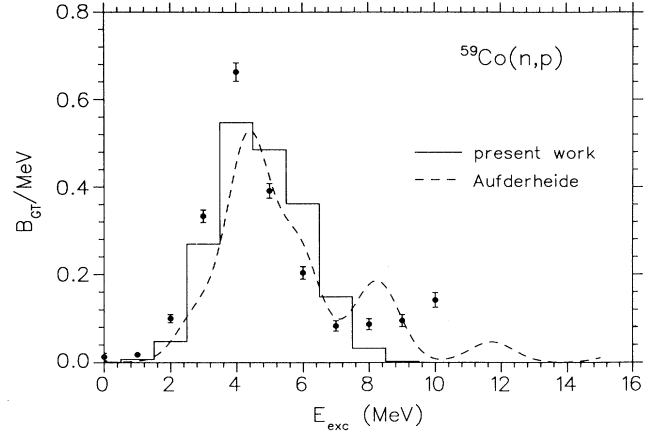

FIG. 11. Comparison of the measured GT strength distribution with model predictions for ^{59}Co. The histogram is the result of calculations described in the text, and the curve is the result of calculations by Aufderheide [20].

was 0.23 for ^{51}V and 0.24 for ^{59}Co. The comparison with the data is shown as the histogram in Figs. 10 and 11.

It is seen that the calculations fit the measured strength distributions reasonably well, although the measured strength is significantly greater than calculations at low excitation energies. This discrepancy would result in an underestimate of stellar electron capture rates, especially at relatively low temperatures. On the other hand, the overall agreement suggests that the model calculations could be used with some confidence to estimate GT distributions for excited states or for unstable nuclei.

A second model calculation has been carried out by Aufderheide [20] using a larger vector space as shown in Table I, with the FPVH effective interaction [21]. The results of this calculation were also broadened to a continuous distribution, and renormalized to the measured GT strength below 8 MeV. In this case, the renormalization required was a factor of 0.31 for V and 0.32 for Co.

A comparison of this result with the experimental data is shown as the dashed curves in Figs. 10 and 11. The quality of the fit to the data is comparable to that for the first calculation. The most noticeable difference is that Aufderheide's calculation with the larger vector space predicts somewhat greater spreading of strength to high excitation energies. The total calculated GT strength is about 25% less than in the first calculation, as a result of the expanded vector space used in this calculation.

B. Spin-dipole transitions

In addition to the GT strength, the multipole analysis provides a quantitative measurement of the cross section for $\Delta L = 1$ transitions which constitute the spin-dipole giant resonance. These transitions correspond to first forbidden beta decay which may make significant contributions to electron capture rates at high temperatures.

The experimental cross section measurements do not permit a direct determination of transition matrix elements as for GT strength however. The spin-dipole giant resonance includes contributions from transitions with $\Delta J = 0$, 1, and 2 which cannot be separately identified in the data. In addition, a non-spin-flip electric dipole component may contribute to transitions with $\Delta J^\pi = 1^-$, even though the non-spin-flip component of the effective interaction is relatively weak at the beam energy used in these measurements.

Unfortunately the DWIA code used here does not permit separate calculations of spin-flip and non-spin-flip components of the transition, but only a reaction cross section for a transition of given J^π transfer to a specified particle-hole configuration. An estimate of the possible magnitude of such effects may be obtained by comparing calculated cross sections with spin-flip transition strengths obtained from a calculation using the program OXBASH [18]. Calculations for transitions to a number of simple particle-hole configurations show that the ra-

TABLE I. Vector spaces used in shell model calculations.

Target	Parent	Daughter
Present results		
^{51}V	$(f_{7/2})^{11}$	$(f_{7/2})^{10}(f_{5/2}p_{3/2}p_{1/2})^1$
^{59}Co	$(f_{7/2})^{15}(f_{5/2}p_{3/2}p_{1/2})^4$	$(f_{7/2})^{14}(f_{5/2}p_{3/2}p_{1/2})^5$
Aufderheide		
^{51}V	$(f_{7/2})^{11,10}(f_{5/2}p_{3/2}p_{1/2})^{0,1}$	$(f_{7/2})^{10,9}(f_{5/2}p_{3/2}p_{1/2})^{1,2}$
^{59}Co	$(f_{7/2})^{15,14}(f_{5/2}p_{3/2}p_{1/2})^{4,5}$	$(f_{7/2})^{15,14,13}(f_{5/2}p_{3/2}p_{1/2})^{4,5,6}$

tio of cross section to spin-flip strength may vary by a factor of 2 for $\Delta J^\pi = 1^-$ transitions to different configurations. In contrast with this, the calculated ratio for $\Delta J^\pi = 0^-$ transitions, for which only the spin-flip component is allowed, is constant to within 10%. This result clearly indicates the possible importance of both spin-flip and non-spin-flip contributions to natural parity transitions.

V. CONCLUSIONS

We have analyzed measurements of the ^{51}V(n,p) and ^{59}Co(n,p) reaction cross sections at 200 MeV to determine the distributions of GT strength for the ground states of these target nuclei. These results are of direct interest in the calculation of electron capture rates in the late stages of evolution of massive stars [20].

The measured distributions have been compared with predictions of a shell model calculation using a restricted vector space and a new effective interaction. These calculations reproduce the overall energy distribution fairly well, although the predicted strength is significantly less than the measured strength at low excitation energies. The magnitude of the total strength is overestimated by a factor of about 4. A second calculation using a larger vector space and a different effective interaction also reproduces the overall strength distribution reasonably well. In this case the total strength is overestimated by a factor of about 3. These model comparisons provide a useful calibration of shell model calculations of GT strength distributions in the mass region $50 < A < 60$, calculations which are an essential ingredient in modeling presupernova collapse of massive stars.

[1] T.N. Taddeucci, C.A. Goulding, T.A. Carey, R.C. Byrd, C.D. Goodman, C. Gaarde, J. Larsen, D. Horen, J. Rapaport, and E. Sugarbaker, Nucl. Phys. **A469**, 125 (1987).

[2] W.P. Alford, R.L. Helmer, R. Abegg, A. Celler, O. Häusser, K. Hicks, K.P. Jackson, G.A. Miller, S. Yen, R.E. Azuma, D. Frekers, R.S. Henderson, H. Baer, and C.D. Zafiratos, Phys. Lett. B **179**, 20 (1986).

[3] H.A. Bethe, G.E Brown, J. Applegate, and J. Lattimer, Nucl. Phys. **A234**, 487 (1979).

[4] K.P. Jackson, A. Celler, W.P. Alford, K. Raywood, R. Abegg, R.E. Azuma, C.K. Campbell, S. El-Kateb, D. Frekers, P.W. Green, O. Häusser, R.L. Helmer, R.S. Henderson, K.H. Hicks, R. Jeppesen, P. Lewis, G.A. Miller, A. Moalem, M.A. Moinester, R.B. Schubank, G.G. Shute, B.M. Spicer, M.C. Vetterli, A.I. Yavin, and S. Yen, Phys. Lett. B **201**, 25 (1988).

[5] G.M. Fuller, W.A. Fowler, and J. Newman, Astrophys. J. **293**, 1 (1985); Astrophys. J. Suppl. **48**, 279 (1982); Astrophys. J. **252**, 715 (1982); Astrophys. J. Suppl. **42**, 447 (1980).

[6] R. Helmer, Can. J. Phys. **65**, 588 (1987).

[7] R.S. Henderson, W.P. Alford, D. Frekers, O. Häusser, R.L. Helmer, K.H. Hicks, K.P. Jackson, C.A. Miller, M.C. Vetterli, and S. Yen, Nucl. Instrum. Methods A **257**, 97 (1987).

[8] R.A. Arndt and L.D. Roper, scattering analysis interaction dial-in (SAID) program (SM90) (unpublished); R.A. Arndt *et al.*, Phys. Rev. D **45**, 3995 (1992).

[9] R. Schaeffer and J. Raynal, computer code DWBA70

(unpublished); J.R. Comfort, computer code DW81 (extended version of DWBA70), Arizona State University (1984).

[10] M.A. Franey and W.G. Love, Phys. Rev. C **31**, 488 (1985).

[11] Computer code MAINX8, T. Cooper (private communication); modified by R.G. Jeppesen (unpublished).

[12] M.C. Vetterli, O. Häusser, W.P. Alford, D. Frekers, R. Helmer, R. Henderson, K. Hicks, K.P. Jackson, R.G. Jeppesen, C.A. Miller, M.A. Moinester, K. Raywood, and S. Yen, Phys. Rev. Lett. **59**, 439 (1987).

[13] A. Klein and N. Auerbach, Phys. Rev. C **30**, 1032 (1984).

[14] M.A. Moinester, Can. J. Phys. **65**, 660 (1987).

[15] M.C. Vetterli, O. Häusser, R. Abegg, W.P. Alford, A. Celler, D. Frekers, R. Helmer, R. Henderson, K.H. Hicks, K.P. Jackson, R.G. Jeppesen, C.A. Miller, K. Raywood, and S. Yen, Phys. Rev. C **40**, 559 (1989).

[16] G.F. Bertsch and I. Hamamoto, Phys. Rev. C **26**, 1323 (1982).

[17] B.E. Vondervecht, W.H. Dickhoff, A. Polls, and A. Ramos, Phys. Rev. C **44**, R1265 (1991).

[18] B.A. Brown, A. Etchegoyen, W.D.M. Rae, and N.S. Godwin, Oxford-Buenos Aires-MSU shell model code (OXBASH), MSUCL Report No. 524, 1986.

[19] B.A. Brown (unpublished).

[20] M. Aufderheide (private communication).

[21] W.A. Richter, M.G.v.d. Merwe, R.E. Julies, and B.A. Brown, Nucl. Phys. **A523**, 325 (1991).